Clinical Cancer Research

Retooling a Blood-Based Biomarker: Phase I Assessment of the High-Affinity CA19-9 Antibody HuMab-5B1 for Immuno-PET Imaging of Pancreatic Cancer

Christian Lohrmann[1,2], Eileen M. O'Reilly[2,3,4], Joseph A. O'Donoghue[5], Neeta Pandit-Taskar[1,2], Jorge A. Carrasquillo[1,2], Serge K. Lyashchenko[2,6,7], Shutian Ruan[1], Rebecca Teng[1], Wolfgang Scholz[8], Paul W. Maffuid[8], Jason S. Lewis[2,6,7,9], and Wolfgang A. Weber[1,2,9]

Abstract

Purpose: In patients with cancer who have an abnormal biomarker finding, the source of the biomarker in the bloodstream must be located for confirmation of diagnosis, staging, and therapy planning. We evaluated if immuno-PET with the radiolabeled high-affinity antibody HuMab-5B1 (MVT-2163), binding to the cancer antigen CA19-9, can identify the source of elevated biomarkers in patients with pancreatic cancer.

Patients and Methods: In this phase I dose-escalating study, 12 patients with CA19-9–positive metastatic malignancies were injected with MVT-2163. Within 7 days, all patients underwent a total of four whole-body PET/CT scans. A diagnostic CT scan was performed prior to injection of MVT-2163 to correlate findings on MVT-2163 PET/CT.

Results: Immuno-PET with MVT-2163 was safe and visualized known primary tumors and metastases with high contrast. In addition, radiotracer uptake was not only observed in metastases known from conventional CT, but also seen in subcentimeter lymph nodes located in typical metastatic sites of pancreatic cancer, which were not abnormal on routine clinical imaging studies. A significant fraction of the patients demonstrated very high and, over time, increased uptake of MVT-2163 in tumor tissue, suggesting that HuMab-5B1 labeled with beta-emitting radioisotopes may have the potential to deliver therapeutic doses of radiation to cancer cells.

Conclusions: Our study shows that the tumor antigen CA19-9 secreted to the circulation can be used for sensitive detection of primary tumors and metastatic disease by immuno-PET. This significantly broadens the number of molecular targets that can be used for PET imaging and offers new opportunities for noninvasive characterization of tumors in patients.

Introduction

Over the last few decades, our understanding of the genetic and molecular underpinnings of pancreatic ductal adenocarcinoma (PDAC) has advanced tremendously; nonetheless, prognosis has remained poor, with an overall 5-year survival rate of 8% (1). About 75% of patients present with locally advanced or metastatic disease and cannot undergo complete tumor resection. In approximately 25% of patients who undergo potentially curative surgery, the 5-year survival rate is still only 20%, suggesting that occult metastatic disease is present at the time of surgery. Thus, the development of technologies that can safely, accurately, and unambiguously detect and stage PDAC remains a critical unmet clinical need (2, 3).

Several imaging modalities are clinically used to detect and stage PDAC, but early detection and accurate staging is limited among these modalities. The shortcomings of CT, PET/CT, MRI, and CT for staging PDAC are well documented—they are particularly poor at identifying small primary lesions and metastases, and in differentiating mass-forming pancreatitis from malignancy (4). Accordingly, novel, more effective imaging technologies are urgently needed.

The remarkable specificity and selectivity of antibodies for cancer biomarkers have made these macromolecules some of the most flexible and adaptable tools in modern medicine. Using

[1]Molecular Imaging and Therapy Service, Department of Radiology, Memorial Sloan Kettering Cancer Center, New York, New York. [2]Weill Cornell Medical College, New York, New York. [3]Department of Medicine, Memorial Sloan Kettering Cancer Center, New York, New York. [4]David M. Rubenstein Center for Pancreatic Cancer Research, Memorial Sloan Kettering Cancer Center, New York, New York. [5]Department of Medical Physics, Memorial Sloan Kettering Cancer Center, New York, New York. [6]Radiochemistry and Imaging Sciences Service, Department of Radiology, Memorial Sloan Kettering Cancer Center, New York, New York. [7]Radiochemistry and Molecular Imaging Probes Core, Memorial Sloan Kettering Cancer Center, New York, New York. [8]MabVax Therapeutics Holdings, Inc. San Diego, California. [9]Molecular Pharmacology Program, Memorial Sloan Kettering Cancer Center, New York, New York.

Note: Supplementary data for this article are available at Clinical Cancer Research Online (http://clincancerres.aacrjournals.org/).

Current address for C. Lohrmann and W.A. Weber: Department of Nuclear Medicine, Technical University Munich, Germany.

J.S. Lewis and W.A. Weber contributed equally to this article.

Corresponding Author: Christian Lohrmann, Technical University Munich, Munich 81675, Germany. Phone: 49-89-4140-4582; E-mail: c.lohrmann@tum.de

Clin Cancer Res 2019;25:7014–23

doi: 10.1158/1078-0432.CCR-18-3667

Translational Relevance

In patients with abnormal biomarker findings, the source of the biomarker in the bloodstream must be located for confirming diagnosis, staging, and therapy planning. We hypothesized that immuno-PET with high-affinity antibodies can identify the source of elevated biomarkers in the blood and thus localize and stage malignant tumors. Our clinical trial reports for the first time that a high-affinity CA19-9 antibody can concentrate more than 184-fold in pancreatic cancer metastases despite the presence of CA19-9 in the plasma with the following implications: (i) immuno-PET targeting CA19-9 is highly promising for noninvasively detecting metastatic pancreatic cancer, an important unmet clinical need; (ii) secreted tumor antigens can be used as targets for imaging (thus far, binding of antibodies to blood antigens was thought to interfere with tumor uptake; and (iii) the high antibody concentration in metastases makes CA19-9 a promising target to selectively deliver cytotoxic agents to pancreatic cancer cells.

antibodies, minute amounts of antigens in the plasma can be detected, making them the main tool for the measurement of blood-based cancer biomarkers. Furthermore, a wide range of antibodies have entered the clinic as novel therapeutics (5).

In the field of nuclear medicine, imaging with radiolabeled antibodies has shown promise for the detection, staging, and characterization of malignant tumors (6). In the present study, we evaluated if a radiolabeled antibody binding to the cancer antigen CA19-9 (Sialyl Lewis A) can localize pancreatic cancer with PET.

CA19-9 levels in the serum are routinely used for diagnosis, risk stratification, and follow-up of PDAC (7). Although CA19-9 is a shed antigen entering the circulation, the concentration is much higher in the tumor tissue, making it a potential target for *in vivo* imaging with radiolabeled antibodies (8, 9). In proof-of-concept preclinical studies, we were able to visualize pancreatic cancer xenograft and orthotopic models of early- and late-stage disease with excellent tumoral uptake and target-to-non-target ratios using the ^{89}Zr-labeled human monoclonal antibody [^{89}Zr]Zr-DFO-HuMab-5B1 (MVT-2163; refs. 8, 10–12). Based on these promising preclinical results, we conducted a first-in-human clinical trial with MVT-2163 PET/CT in CA19-9–positive malignancies (NCT02687230).

HuMab-5B1 is a fully human IgG1 lambda antibody identified from peripheral lymphocytes in a patient following immunization with a Sialyl Lewis A (sLe^a)-KLH vaccine (13). HuMab-5B1 binds the sLe^a epitope on the cancer antigen CA19-9 with exceptional binding affinity (K_d = 0.14 nmol/L) and is highly internalized. Binding is also highly specific with no cross-reactivity for related carbohydrates such as Lewis A, Lewis X, or Lewis Y (14). In addition, the HuMab-5B1 antibody has shown potent complement- and antibody-dependent cytotoxicity both *in vitro* and in murine models of numerous cancers, including PDAC (14).

Patients and Methods

Trial design

The study was a phase I dose-escalation study with the goal of determining the feasibility and safety of PET/CT imaging with MVT-2163 for the detection of metastatic CA19-9–positive malignancies. Because the injected mass of a radiolabeled antibody can significantly affect its uptake by tumor and normal organs, groups of patients were planned to be injected with targeted antibody masses ranging from 3 to 50 mg in a standard "3+3" dose-escalation design. Dose escalation was to end in the event of unacceptable toxicity [common terminology criteria for adverse events (CTCAE) grade 2 or higher], when image quality deteriorated, or an injected mass of 50 mg had been reached. At the highest dose level, three additional patients were included to better determine the distribution of antibody uptake in tumor lesions and normal organs. The study was approved by the local Institutional Review Board and conducted in accordance with the Declaration of Helsinki. Informed consent was obtained from all patients after the nature and possible consequences of the study were explained.

MVT-2163 preparation

The fully human HuMab-5B1 antibody was manufactured for MabVax Therapeutics Holdings, Inc. by Patheon Biologics under current good manufacturing practice guidelines and supplied in sterile vials to MSK. The radiolabeled HuMab-5B1 antibody was manufactured at MSK in compliance with the requirements specified in the Chemistry, Manufacturing, and Controls section of an FDA-acknowledged IND (FDA IND No. 126,425). The preparation process involved conjugating clinical-grade HuMab-5B1 with a bifunctional chelator, p-SCN-deferoxamine (DFO; Macrocyclics), followed by radiolabeling with ^{89}Zr, a radiometal positron emitter with a 78.4-hour radioactive half-life. The conjugation and radiolabeling were performed using methodology previously described (15). Radiolabeling with ^{89}Zr was chosen based on its metallo-radionuclide's favorable properties such as mild radiolabeling conditions, positron emission, and sufficiently long radioactive half-life to allow for imaging with radiolabeled antibodies (16). Twelve MVT-2163 batches were prepared in total. The mean radiolabeling yield was 64% (range, 44%–91%), and the mean specific activity was 104.71 MBq/mg (range, 67.71–163.17 MBq/mg). The mean radionuclide incorporation in the MVT-2163 final drug product was 99.8% (range, 98.4%–100%), as measured by radio-TLC. The mean antibody monomer content in the final MVT-2163 drug product was 99.4% (range, 88.95%–100%), as measured by SEC-HPLC. The mean percent immunoreactive fraction was 90.9% (range, 85.5%–96.4%), as determined by the live antigen expressing cell immunoreactivity Lindmo assay (17).

As part of the antibody mass escalation scheme, the first three patients were administered a targeted amount of 3 mg of the radiolabeled antibody only, as a single injection. The three patients in the second cohort were each administered a total targeted amount of 20-mg antibody, and six patients in the third cohort were each administered a total targeted amount of 50-mg antibody. For these subjects, a separate syringe containing a targeted amount of 17 and 47 mg, respectively, of unlabeled HuMab-5B1 was dispensed and administered prior to MVT-2163.

Patients

Key eligibility criteria for study inclusion were histologically confirmed, locally advanced metastatic disease known to express CA19-9, and at least one tumor lesion on baseline CT measuring $\geq$ 2 cm and an Eastern Cooperative Oncology Group performance status of 0 to 2. Twelve consecutive patients with CA19-9–positive metastatic malignancies (11 PDAC, 1 CA19-9–producing tumor

of unknown origin with peritoneal carcinomatosis) were injected i.v. over 20 minutes with a mean activity of 169 ± 7 MBq MVT-2163 labeled to a fixed antibody target mass of 3 mg. Cohort 1 received MVT-2163 only without nonradiolabeled Humab-5B1. In cohorts 2 and 3, the nonradiolabeled HuMab-5B1 was injected 1 to 4 hours prior to administration of the radiolabeled Humab-5B1 over 60 minutes. No premedications were administered. Patients were monitored clinically for at least 90 minutes after injection of the radiolabeled antibody before discharge for any reactions or adverse events, which were graded per CTCAEs 4.0.

Imaging

All patients underwent a total of four PET/CT scans (field of view: base of the skull to upper thighs) on day 1 (day of injection), day 2, day 4 ± 1, and day 7 ± 1. Scans were acquired on a GE Discovery 710 scanner in three-dimensional mode (first scan 3, second scan 4, third scan 5, and the fourth scan 7 minutes per bed position). PET/CT scans were obtained with a low-dose CT for attenuation correction (first three scans with 10-mA current; last scan with 80-mA current). Images were reconstructed using ordered-subset expectation maximization parameters (two iterations; 16 subsets) and attenuation correction.

A diagnostic CT scan of the chest, abdomen, and pelvis was performed in all patients within 4 weeks prior to injection of MVT-2163 and was used to correlate findings on MVT-2163. Criteria for metastatic lymph nodes on CT were a short-axis diameter of more than 1 cm or otherwise not explainable growth when compared with prior CT scans. Peritoneal nodules or infiltration of the peritoneum by soft tissue was considered as indication of peritoneal carcinomatosis. Poorly defined or newly hypodense liver lesions on contrast-enhanced CT images during the portal venous phase were considered as liver metastases. Multiple round pulmonary nodules or newly developed solitary pulmonary nodules were considered as lung metastases. Criteria for osseous metastases were osseous destructions or newly developed lytic or sclerotic lesions in the skeleton.

Whole-body and serum clearance measurements

Whole-body clearance was derived from serial measurements of count rate using a 12.7-cm-thick (5-inch) sodium iodide NaI (Tl) scintillation detector at a fixed geometry (3 m from probe to patient). Probe measurements were made following MVT-2163 infusion before and after first voiding, and at the times of PET imaging. Background-corrected geometric mean count rates were normalized to the immediate postinfusion value to yield relative retained activities. To determine clearance from the circulation, blood samples were taken at 15, 30, and 90 minutes after infusion and subsequently at the times of PET imaging. Serum activity concentration was measured with a NaI (Tl) gamma well-type detector (Wallac Wizard 1480 automatic gamma counter, PerkinElmer) and converted to percent injected activity/liter (% IA/L).

Image analysis

Volumes of interest (VOI) were drawn on PET/CT images within normal tissues with visible uptake of MVT-2163 (typically liver, kidney, spleen, lung, gut, and vertebral bone) and converted to activity concentration per unit mass (kBq/g), assuming a density of 1 g/mL for all tissues except lung (density taken to be 0.3 g/mL) and bone (density taken to be 1.9 g/mL). Focal tracer uptake not explained by activity in the blood pool or excreted activity in liver and gastrointestinal tract was considered abnormal and suspicious for malignancy. In addition, tracer uptake of lesions as well as for normal organs was quantified by standardized uptake values normalized to patients' body weight (SUV). Maximum SUVs were used for lesions to decrease the impact of partial volume averaging. Mean SUVs were used for normal tissues. Radiation dosimetry was calculated from the imaging and blood radioactivity data as described in detail in the Supplementary Methods.

Statistical analysis

Quantitative results are reported by mean values ± one SD. Correlations between quantitative parameters were analyzed by Spearman rank correlation. A P value of less than 0.05 was considered as statistically significant.

Results

Patient safety

Injection of MVT-2163 as a single agent and in combination with the nonradiolabeled HuMab-5B1 antibody was well tolerated at all dose levels. Six patients had no side effects, and six patients demonstrated mild to moderate side effects with chills, nausea, fever, hot flashes, and hypertension after injection (three CTCAE grade 1, two CTCAE grades 1 and 2, and one CTCAE grades 1 and 3). All side effects resolved on the day of the injection, with some requiring supportive medication.

Pharmacokinetics and biodistribution of MVT-2163

The clearance of MVT-2163 from whole body and serum conformed to mono- and biexponential curves, respectively, with no statistically significant difference between antibody mass doses (Fig. 1). The set of kinetic parameters for all patients including biological whole-body half-life is provided in Supplementary Table S1. As is typical for radiolabeled antibodies, the kinetic evolution of normal tissue uptake featured a gradual redistribution from blood pool to parenchymal tissues and hepatobiliary excretion routes. The highest normal tissue uptake observed was in liver and, to a lesser extent, spleen. Generally, uptake in other parenchymal organs (kidney, lung) was relatively low. Diffuse low-level uptake in bone was seen in some but not all patients. Maximal gut uptake was typically seen between 24 and 48 hours after injection.

Radiation dosimetry of MVT-2163

The full set of residence times for all patients is provided in Supplementary Table S2. The corresponding absorbed dose estimates are shown in Supplementary Table S3 and summarized graphically in Supplementary Fig. S1. The normal tissues experiencing the highest absorbed doses were liver (mean 3.3 ± 1.2 mGy/MBq) and spleen (mean 1.4 ± 0.7 mGy/MBq), reflecting their higher observed uptake. The average effective dose was 0.51 mSv/MBq ± 0.13. There was no statistically significant correlation between antibody mass dose and normal tissue absorbed dose. However, there was a nonsignificant trend for reduced absorbed doses to liver and spleen at higher antibody mass doses (Fig. 1A).

Lesion targeting of MVT-2163

Primary PDAC and known metastases were visualized with high contrast (Figs. 2 and 3C). Importantly, we did not only

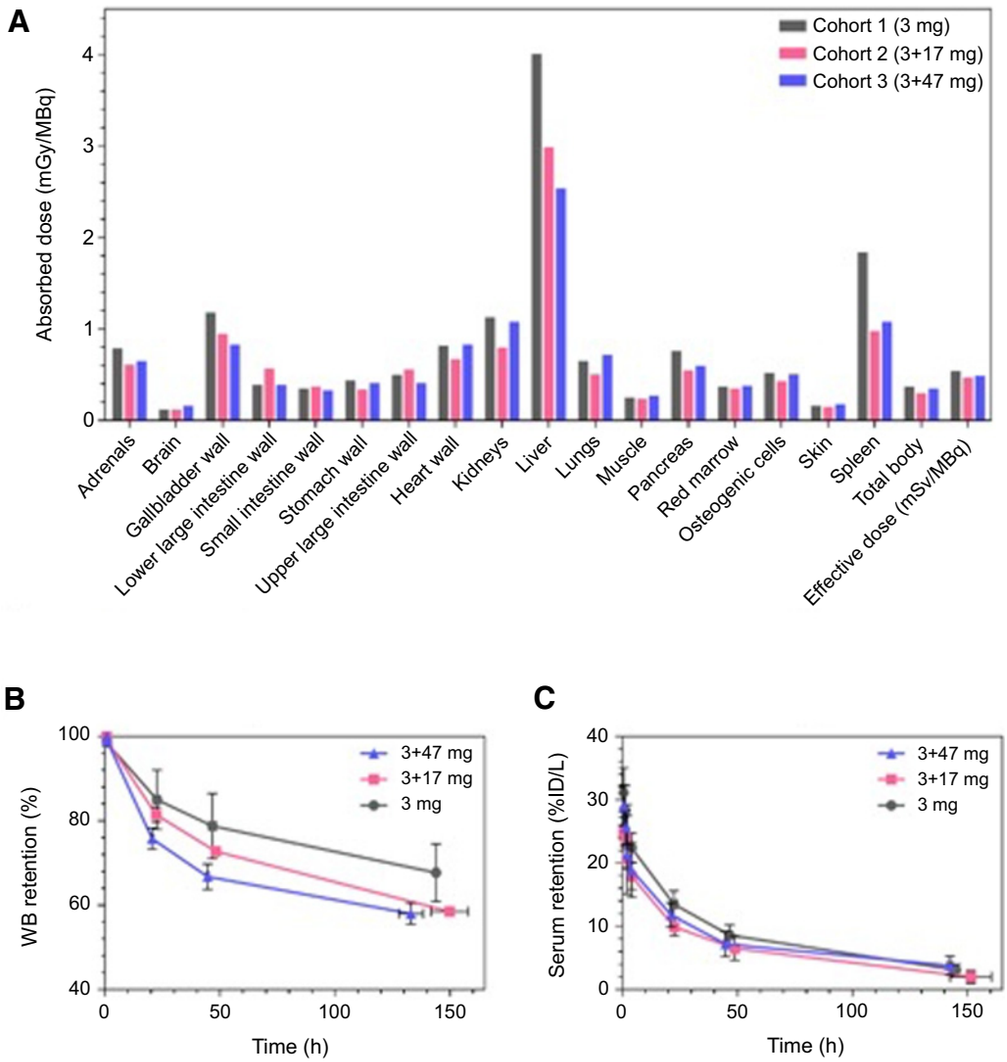

Figure 1.

MVT-2163 absorbed dose estimates. **A,** Selected median values for the three mass dose cohorts show a nonsignificant trend of reduced liver and spleen doses for higher antibody masses. Clearance from (**B**) whole body and (**C**) serum generally conformed to mono- and biexponential curves, respectively, with no statistically significant difference between antibody mass doses.

observe uptake of MVT-2163 by metastases known from conventional imaging studies, but also intense radiotracer uptake in subcentimeter lymph nodes located in typical metastatic sites of PDAC, which were not abnormal on routine clinical imaging studies (Supplementary Fig. S2). Strikingly, at least one additional lesion was seen on MVT-2163 5B1 PET/CT in each of the 12 patients.

Uptake of HuMab-5B1 was analyzed quantitatively for a total of 78 lesions. Focal radiotracer uptake continuously increased to day 7 with an average SUV_{max} for all three antibody levels combined at days 1, 2, 4, and 7 of 3.51 ± 2.58, 9.3 ± 14.3, 12.6 ± 14.5, and 16.5 ± 17.3, respectively. At the lowest antibody mass level (3 mg) in the absence of a preinjection of the unlabeled 5B1 antibody, the liver showed high radioactivity uptake at day 7 (average SUV 19.7 ± 2.9; Fig. 3A and B), which limited the detection of liver metastases. However, preinjection of 17 and 47 mg of unlabeled HuMab-5B1 significantly decreased liver uptake ($r = -0.61$, $P = 0.014$, Fig. 3). Most of the decrease in liver uptake occurred between the 3- and 20-mg total antibody mass with a further mild decrease between the 20- and the 50-mg antibody mass. In the group of patients who received 47-mg cold antibody, liver metastases seen on conventional imaging demonstrated clear focal radiotracer uptake with tumor-to-liver ratios of up to 8.5, allowing for excellent visualization of subcentimeter liver metastases (Fig. 3B and C). No statistically significant correlation between antibody mass and lesion SUVs existed (Fig. 2A). On day 7, lesion SUV_{max} was as high as 101.4 g/mL, indicating that the radioactivity was concentrated more than 100-fold in the lesions when compared with a homogenous distribution throughout the body. The average lesion-to-blood ratio on day 7 was 18.4, and 50% of the lesions demonstrated a lesion-to-blood ratio of more than 10 (Fig 4).

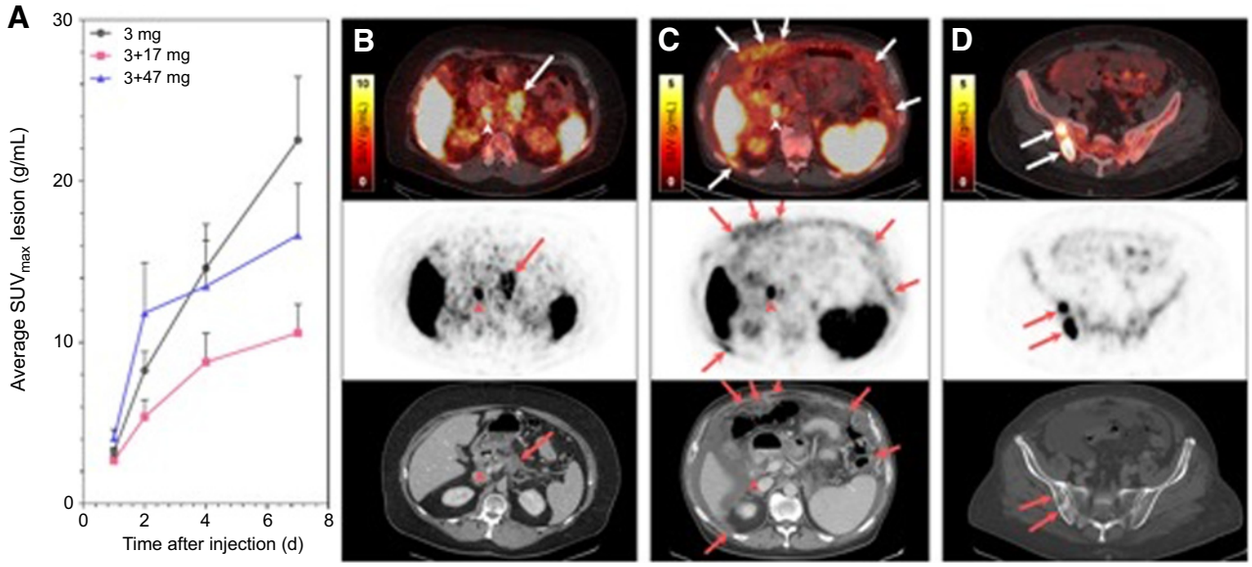

Figure 2.

MVT-2163 PET/CT detects primary pancreatic tumors and metastatic disease. **A,** Average lesion uptake of MVT-2163 over time for the three antibody masses. Error bars show the SEM. There is no clear correlation between antibody dose and lesion SUVs. **B,** Fifty-four-year-old male with locally advanced unresectable pancreatic adenocarcinoma, treated with chemotherapy and stereotactic body radiation, presents with rising CA19-9 antigen levels of 2,255 U/mL. Axial fused PET/CT image (top row) and axial PET image (middle row) after injection of 3-mg MVT-2163 demonstrates uptake in the primary pancreatic tumor (arrow) and in the portacaval region (arrowhead). Foci of uptake on PET correlate with ill-defined pancreatic mass (arrow) and adenopathy seen on diagnostic CT (arrowhead) performed 3 weeks prior (lower row). Diffuse nonspecific uptake is seen on PET in the visualized regions of the liver and spleen with no correlate on diagnostic CT. **C,** In a 65-year-old male with metastatic pancreatic adenocarcinoma (rising CA19-9 antigen levels of 287 U/mL), axial fused PET/CT image (top row) and axial PET image (middle row) after injection of 17-mg nonradiolabeled 5B1 antibody and 3 mg of MVT-2163 demonstrate multiple widespread foci of uptake in the region of the peritoneum (arrows) and uptake in the portacaval region (arrowhead). Foci of uptake on PET correlate with widespread peritoneal carcinomatosis (arrows) and portacaval adenopathy (arrowhead) seen on diagnostic CT performed 1 day prior (lower row). **D,** In the same patient, axial fused PET/CT image (top row) and axial PET image (middle row) demonstrate foci of uptake in the right iliac bone (arrows). Foci of uptake on PET correlate with a large mixed lytic/sclerotic bone metastasis on diagnostic CT (arrows) performed 1 day prior (lower row).

CA19-9 values varied from 14 to 6,277 U/mL (average: 1,403 U/mL). There was a statistically significant, but weak positive correlation between CA19-9 and lesion SUV at day 7 ($r = 0.28$, $P = 0.014$, Fig. 5). No statistically significant correlations between CA19-9 values and blood and liver SUVS at day 7 were observed ($r = -0.51$, $P = 0.09$ and $r = 0.45$, $P = 0.15$, respectively).

One patient with metastatic PDAC never had elevated CA19-9 levels in the blood during the course of the disease (CA19-9 14 U/mL at the time of imaging). However, CT detected several metastases, which were positive on the MVT-2163 PET.

Discussion

This is the first clinical study of PET/CT imaging of CA19-9–positive malignancies with a fully human ^{89}Zr-labeled anti–CA19-9 antibody. Our clinical results confirm the excellent targeting of CA19-9–positive malignancies with MVT-2163 in preclinical studies and indicate that MVT-2163 is promising for the detection and staging of CA19-9–positive malignancies. In the past, a few radiolabeled antibodies have been evaluated to target CA19-9–positive malignancies in humans, mainly using the gamma emissions of ^{131}I (18, 19). Due to the inherent limitations in imaging and radiation dose properties, the use of ^{131}I has been discontinued. ^{89}Zr, however, is a positron emitter that can be imaged by PET and provides drastically higher sensitivity and spatial resolution than gamma camera imaging with ^{131}I. A further advantage of PET is its ability to easily measure activity concentrations in the tumor and normal organs.

The herein presented first-in-human data indicate that MVT-2163 PET/CT is safe and highly promising for the detection of CA19-9–positive malignancies. A significant fraction of the patients demonstrated very high, and over time increased, uptake of MVT-2163 in the tumor tissue (SUV_{max} up to ~101.4 g/mL and average tumor-to-blood ratios of 18.4 on day 7 ± 1), confirming the high tumor uptake found in animal models (8), and suggesting that HuMab-5B1 may deliver therapeutic doses to PDAC when labeled with beta-emitting radioisotopes, similar to somatostatin receptor or prostate-specific membrane antigen-targeting radioligands (20, 21). Indeed, it has been shown in preclinical pretargeting studies that derivatives of ^{177}Lu and HuMab-5B1 can rapidly and specifically deliver a radiotherapeutic payload to tumor tissue (10). Clinically, [^{177}Lu]Lu-CHX-A″-DTPA-5B1 (MVT-1075, NCT03118349) is under study in an open-label, nonrandomized dose-escalation trial to evaluate its safety and dosimetry and to determine the MTD in subjects with CA19-9–positive malignancies. In addition to this potential use as a theranostic agent, HuMab-5B1 has also demonstrated therapeutic efficacy as a "naked antibody" in animal models of pancreatic cancer (14) and is currently being tested in a phase I clinical trial (MVT-5873, NCT02672917). Thus, imaging with MVT-2163 provides a unique way to study tumor uptake of HuMab-5B1 that could be used not only for imaging, but also for guiding CA19-9–directed therapy.

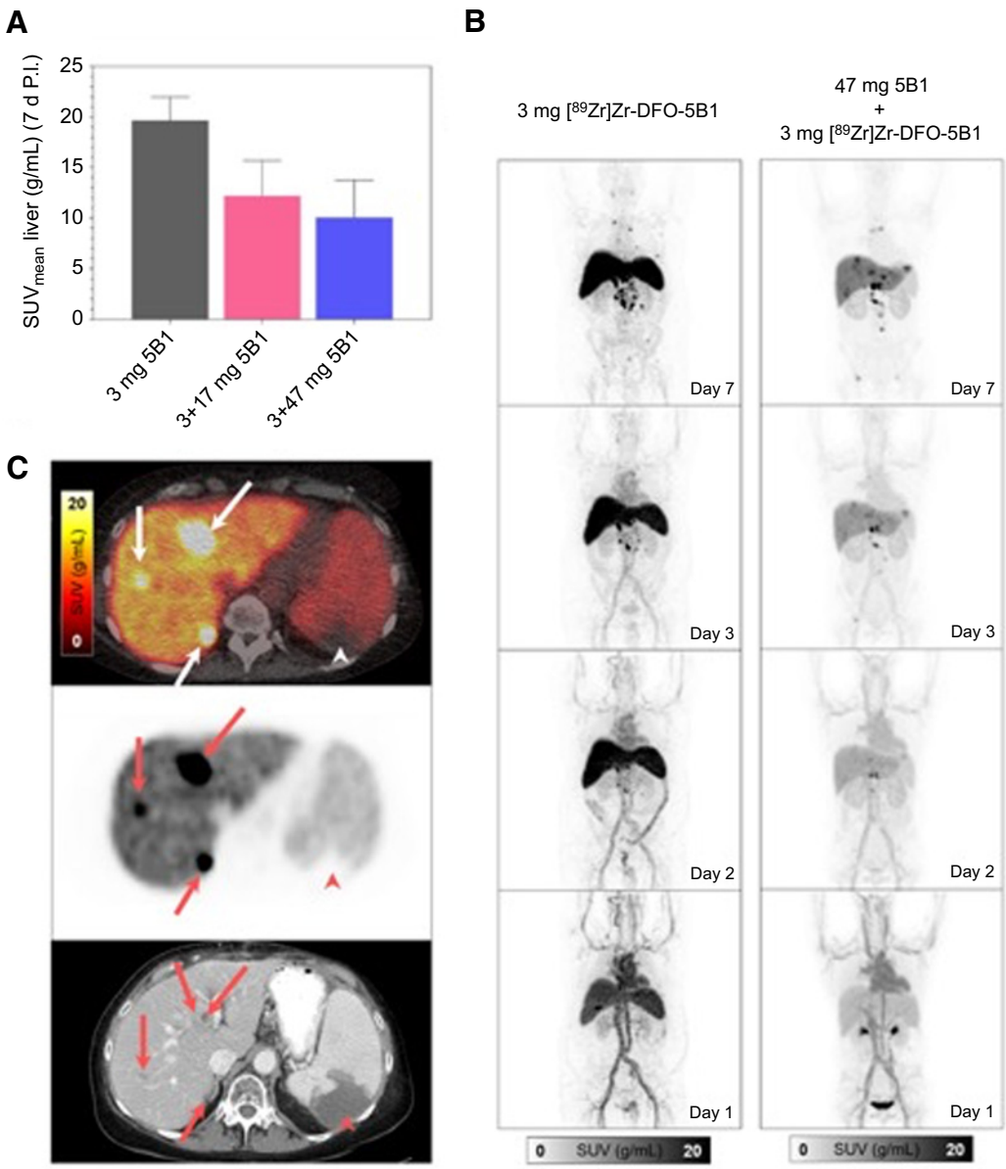

Figure 3.

Radiotracer uptake of normal liver parenchyma (SUV_{mean}) depending on the antibody mass injected. **A,** There is a reduction in liver uptake of radioactivity with increasing antibody mass (error bars show one SD). **B,** Maximum-intensity projection image demonstrates the effect in a patient injected with 3-mg antibody (left) and a (different) patient injected with 47-mg HuMab 5B1 antibody 2 hours before injection of 3-mg radiolabeled HuMab 5B (right). **C,** Fused PET/CT, PET, and contrast-enhanced CT of PDAC liver metastases in a patient who received 47 mg of HuMab 5B1 before injection of the radiolabeled antibody. Small liver metastases measuring less than 5 mm (red arrows) are visualized with high contrast. SUV values were 101.4, 70.7, and 53.4 g/mL, respectively. Arrowhead indicates splenic infarct.

In the presented study, preinjection of 17- and 47-mg unlabeled HuMab-5B1 decreased liver uptake, resulting in improved visualization of liver metastases. There was also a minor further decrease of liver uptake in patients that received 47 mg as compared with 17-mg unlabeled antibody. In addition, SUVs for lesions were higher in patients that had received 47-mg cold antibody, but this difference was not statistically significant. These results slightly favor MVT-2163 PET/CT imaging with preinjection of 47-mg nonradiolabeled HuMab-5B1. Importantly, CA19-9 concentrations in the serum (which varied several hundred-fold) had no relevant effect on tumor uptake of MVT-2163 and did also not significantly affect blood and liver activity concentrations. This confirmed our preclinical observation that high-contrast imaging of CA19-9–positive tumors was feasible even in the presence of significant amounts of CA19-9 in the circulation (8, 12).

Lesion uptake was quantified by SUV_{max} while SUV_{mean} was used for normal tissue uptake. This was done because SUV_{mean} may underestimate lesion uptake due to partial volume averaging effects, especially for smaller lesions.

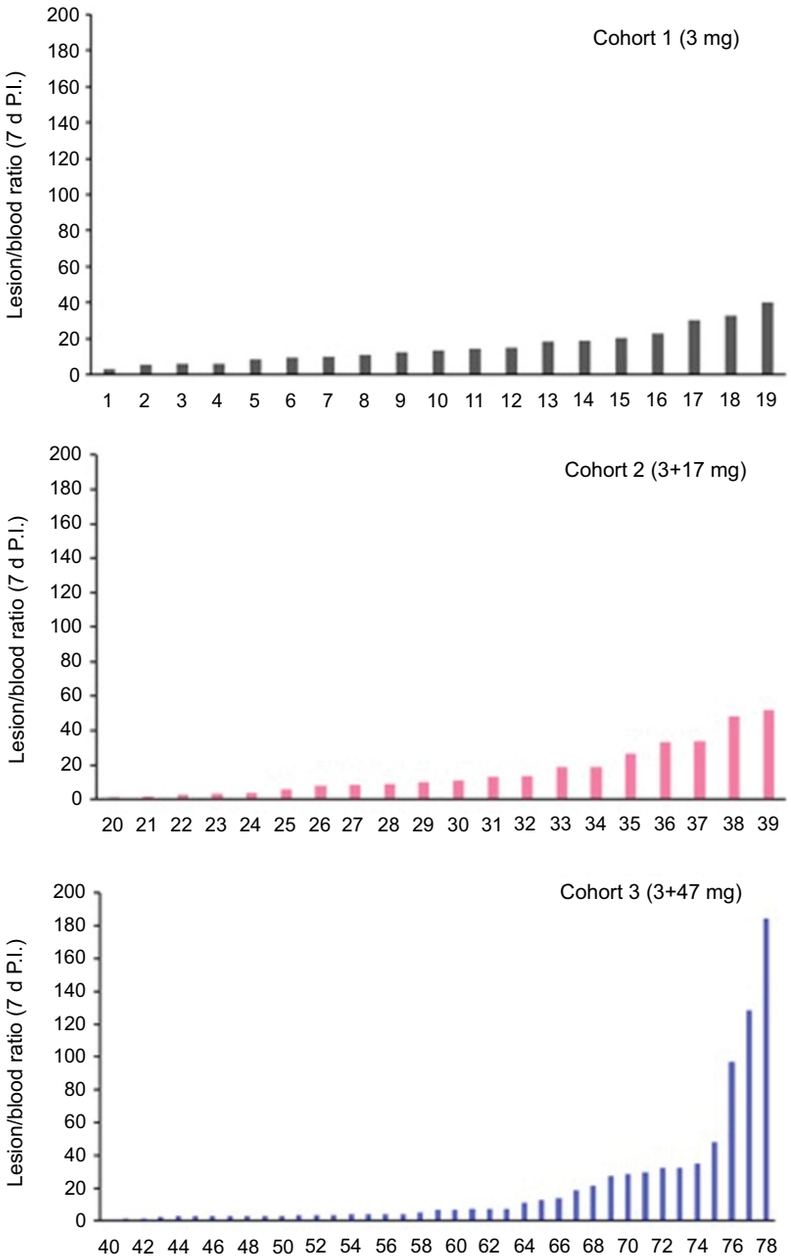

Figure 4.
Lesion/blood ratio in lesions on day 7 for the three patient cohorts. The average lesion-to-blood ratio on day 7 was 18.4, and 50% of all lesions demonstrated a lesion-to-blood ratio of more than 10.

Whereas, in contrast, normal organ VOI are large enough that partial volume effects are minimal. However, it could be argued that such an approach may produce misleadingly high values of tumor-to-liver ratio. In Supplementary Fig. S3, we provide an alternate version of Fig. 3A that illustrates the mass dependency of liver SUV_{max}. All values are greater, as expected, but the same trend of decreasing liver uptake with increasing mass dose is apparent. Also, as expected, tumor SUV_{max} to liver SUVmax ratios are less than tumor SUV_{max} to liver SUV_{mean} ratios. For example, a tumor-to-liver ratio of 8.5 as quoted in results would be 5.5 when expressed as the ratio of SUV_{max}.

MVT-2163 PET/CT did not only show obvious metastases known from conventional imaging studies, but also intense radiotracer uptake in subcentimeter lymph nodes located in typical metastatic sites of PDAC that were not abnormal on routine clinical imaging studies. This aspect warrants future studies, because lymphatic dissemination of small clusters of tumor cells is a well-established feature of PDAC and a major challenge for PDAC treatment (22).

Although CA19-9 is the most commonly used serum tumor marker for PDAC, it has several well-established limitations (7). CA19-9 is not specific for PDAC, but is also released by several other gastrointestinal malignancies. Furthermore, benign medical conditions such as biliary obstruction and pancreatitis can cause markedly elevated CA19-9 levels. The sensitivity and specificity of CA19-9 for detection of resectable (stage I–II) PDAC are both approximately 70%, and sensitivity decreases

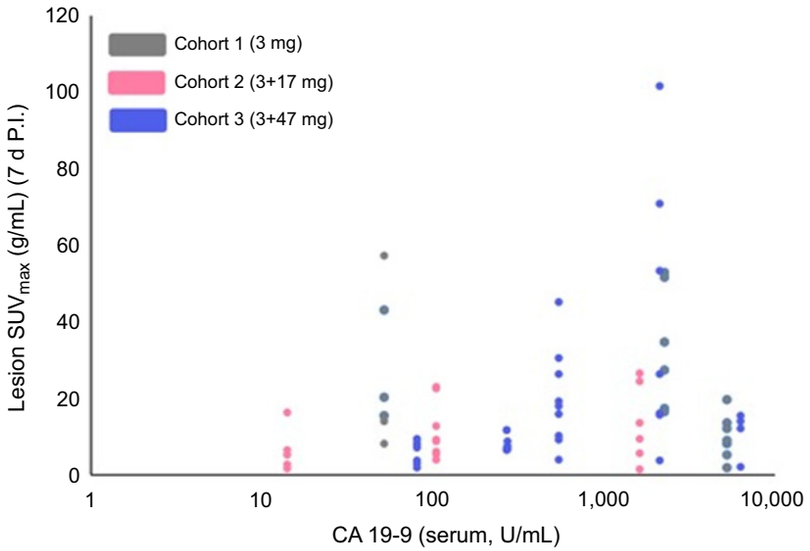

Figure 5.
Influence of serum CA19-9 levels on radioactivity concentrations in lesions on day 7. CA19-9 values varied from 14 to 6,277 U/mL (average: 1,403 U/mL). There was a statistically significant, but weak positive correlation between CA19-9 and lesion SUV at day 7 ($r = 0.28$, $P = 0.014$).

with decreasing tumor size (23). CA19-9–directed imaging has the potential to overcome several of these limitations. The location of tracer uptake on the imaging studies should allow for differentiation of PDAC and other malignancies. We also expect the distribution of tissue uptake of MVT-2163 to be diffuse in inflammatory conditions, whereas PDACs and their metastases demonstrate focal tracer uptake. Furthermore, in the present study, tumor visualization occurred over a broad range of serum CA19-9 levels, and there was no clear impact of serum CA19-9 on tumor SUVs. We also included one patient with metastatic PDAC but with no elevation of CA 19-9. Interestingly, in this patient, several metastases (known from CT imaging) showed uptake of MVT-2163 on the PET images, suggesting that immuno-PET can be more sensitive than analysis of CA19-9 levels in the serum.

The following limitations of our study and of immuno-PET in general should be noted. In this phase I trial in patients with advanced pancreatic cancer, we do not have histopathologic confirmation that the small lymph nodes seen on MVT-2163 PET/CT were due to metastases. It is conceivable that MVT-2163 uptake in those lymph nodes was due to secreted CA19-9 that had entered the lymphatic system. Assessing the specificity of MVT-2163 PET/CT for detection of lymph node metastases will therefore require future studies in patients scheduled to undergo lymph node dissection for pancreatic cancer.

It needs also to be emphasized that previous approaches targeting soluble antigens, such CA 19-9, CEA, or MUC1, did eventually not improve sensitivity of cancer staging when compared with anatomical imaging despite initially promising results (19, 20, 24). Advantages of MVT-2163 PET/CT are the high affinity and specificity MVT-2163 for CA-9 as well as the higher sensitivity and spatial resolution of PET as compared with SPECT and planar scintigraphy. However, rigorous prospective studies are required to determine if these strengths of MVT-2163 PET/CT can overcome the well-documented limitations of immunoscintigraphy observed in previous studies.

A practical limitation of imaging with ^{89}Zr-labeled antibodies, including MVT-2163, is the relatively long timeframe required to reach high tumor uptake (6). In the present study, we observed a continued increase in tumor uptake of MVT-2163 for 7 days, whereas tumor uptake of small molecules such as ^{18}F-fluorodeoxyglucose typically plateaus within a few hours after injection. The slow uptake and excretion of antibodies is a significant logistic problem for the clinical use of MVT-2163 PET/CT. It also results in an effective dose of 0.51 mSv/MBq which is in the range of effective doses reported for other ^{89}Zr-labeled antibodies such as the Her2 antibodies ^{89}Zr-Trastuzumab, 0.48 mSv/MBq and ^{89}Zr-Pertuzumab, 0.54 mSv/MBq, and the PSMA antibody ^{89}Zr-J591, 0.38 mSv/MBq (25–27), but several-fold higher than for ^{18}F-fluorodeoxyglucose (0.029 mSv/MBq; ref. 28).This high radiation exposure will likely limit the use of MVT-2163 for screening and early detection of PDAC with currently available PET/CT systems.

However, a new generation of PET/CT systems with 40 times higher sensitivity has recently been introduced (29). With such systems, a scan with MVT-2163 can be performed with less radiation exposure than a ^{18}F-fluorodeoxyglucose PET/CT scan with a current generation scanner. Even with the current systems, radiation exposure is much less of an issue for preoperative staging of patients with a diagnosis of PDAC. Because of the high likelihood of clinically occult disease in pancreatic cancer patients, the benefits of more accurate staging will almost certainly outweigh the possible radiation risks. Complete tumor resection is the only potentially therapy for pancreatic adenocarcinomas. This requires major surgery that is associated with significant risks for perioperative complications as well as long-term morbidity. According to a recent meta-analysis, 42% of patients with resectable pancreatic cancer on CT imaging are found to have unresectable disease at the time of surgery (30). Even after histologically complete tumor resection, 5-year survival is only about 25% (31). This clearly indicates that there is significant unmet clinical need for better imaging technologies to stage pancreatic cancer which may well justify the logistic challenges of immuno-PET.

In conclusion, our study shows that a tumor antigen secreted to the circulation can potentially be used for sensitive detection of primary tumors and metastatic disease by immuno-PET. This significantly broadens the number of molecular targets that can be used for PET imaging and provides new opportunities for noninvasive characterization of tumors in patients. Specifically,

targeting CA19-9 with MVT-2163 PET/CT is promising for the detection and staging of PDAC and other CA19-9–positive malignancies. Future studies that more comprehensively interrogate the role of immuno-PET with MVT-2163 in pancreatic cancer by correlation with histologic findings are warranted.

Disclosure of Potential Conflicts of Interest

E.M. O'Reilly is an employee/paid consultant for Celgene, CytomX Therapeutics, Sobi, BioLineRx, Merck and Targovax, and reports receiving commercial research grants from Celgene, MabVax Therapeutics, Actabiologica and AstraZeneca. N. Pandit-Taskar is an employee/paid consultant for Progenics and Actinium Pharma. J.A. Carrasquillo is an employee/paid consultant for Y-mabs, reports receiving commercial research grants from Genentech, Gilead, Regeneron, and Ludwig, and reports receiving other commercial research support from Bayer. W. Scholz is an employee/paid consultant for and holds ownership interest (including patents) in MabVax Therapeutics. P.W. Maffuid is an employee/paid consultant for MabVax Therapeutics Holdings, Inc. J.S. Lewis reports receiving commercial research grants from MaxVax Therapeutics Inc. W.A. Weber is an employee/paid consultant for Ipsen. No potential conflicts of interest were disclosed by the other authors.

Authors' Contributions

Conception and design: C. Lohrmann, E.M. O'Reilly, J.A. O'Donoghue, J.A. Carrasquillo, S.K. Lyashchenko, P.W. Maffuid, J.S. Lewis, W.A. Weber
Development of methodology: C. Lohrmann, J.A. O'Donoghue, N. Pandit-Taskar, J.A. Carrasquillo, S.K. Lyashchenko, S. Ruan, J.S. Lewis, W.A. Weber
Acquisition of data (provided animals, acquired and managed patients, provided facilities, etc.): C. Lohrmann, E.M. O'Reilly, J.A. O'Donoghue, N. Pandit-Taskar, R. Teng, J.S. Lewis
Analysis and interpretation of data (e.g., statistical analysis, biostatistics, computational analysis): C. Lohrmann, E.M. O'Reilly, J.A. O'Donoghue, N. Pandit-Taskar, S. Ruan, P.W. Maffuid, J.S. Lewis, W.A. Weber
Writing, review, and/or revision of the manuscript: C. Lohrmann, E.M. O'Reilly, J.A. O'Donoghue, N. Pandit-Taskar, J.A. Carrasquillo, S.K. Lyashchenko, W. Scholz, P.W. Maffuid, J.S. Lewis, W.A. Weber
Administrative, technical, or material support (i.e., reporting or organizing data, constructing databases): C. Lohrmann, J.A. Carrasquillo, S.K. Lyashchenko, R. Teng
Study supervision: C. Lohrmann, E.M. O'Reilly, J.S. Lewis, W.A. Weber

Patent

HuMab-5B1 and ^{89}Zr-DFO-HuMab-5B1 are protected under US patent number US 9,475,874 and worldwide applications are pending. WS is an inventor on the 5B1 patent; all rights are assigned to MabVax Therapeutics, Inc.

Acknowledgments

We thank the pharmacy, nursing, and technologist staff of the Molecular Imaging and Therapy Service in the Department of Radiology at Memorial Sloan Kettering Cancer Center for their continued support and Dr. Lukas Carter at MSK for help in preparation of this article.

The study was funded in part by MabVax Therapeutics, Inc. and by the David M. Rubenstein Center for Pancreatic Cancer Research at Memorial Sloan Kettering Cancer Center. Furthermore, the authors gratefully acknowledge the Memorial Sloan Kettering Cancer Center Radiochemistry and Molecular Imaging Probe Core (NIH grant P30 CA008748), and the NCI (R01 CA222049-01A1 to C. Lohrmann, J.S. Lewis, and W.A.Weber, R35 CA232130 to J.S. Lewis and HHSN261201300060C grant to W. Scholz) for additional support.

The costs of publication of this article were defrayed in part by the payment of page charges. This article must therefore be hereby marked *advertisement* in accordance with 18 U.S.C. Section 1734 solely to indicate this fact.

Received November 12, 2018; revised May 14, 2019; accepted September 6, 2019; published first September 20, 2019.

References

1. Siegel RL, Miller KD, Jemal A. Cancer statistics, 2018. CA Cancer J Clin 2018;68:7–30.
2. Neoptolemos JP, Kleeff J, Michl P, Costello E, Greenhalf W, Palmer DH. Therapeutic developments in pancreatic cancer: current and future perspectives. Nat Rev Gastroenterol Hepatol 2018;15:333–48.
3. Ryan DP, Hong TS, Bardeesy N. Pancreatic adenocarcinoma. N Engl J Med 2014;371:1039–49.
4. Treadwell JR, Zafar HM, Mitchell MD, Tipton K, Teitelbaum U, Jue J. Imaging tests for the diagnosis and staging of pancreatic adenocarcinoma: a meta-analysis. Pancreas 2016;45:789–95.
5. Reichert JM, Valge-Archer VE. Development trends for monoclonal antibody cancer therapeutics. Nat Rev Drug Discov 2007;6:349–56.
6. Moek KL, Giesen D, Kok IC, de Groot DJA, Jalving M, Fehrmann RSN, et al. Theranostics using antibodies and antibody-related therapeutics. J Nucl Med 2017;58(Suppl 2):83s–90s.
7. Scara S, Bottoni P, Scatena R. CA 19-9: Biochemical and clinical aspects. Adv Exp Med Biol 2015;867:247–60.
8. Viola-Villegas NT, Rice SL, Carlin S, Wu X, Evans MJ, Sevak KK, et al. Applying PET to broaden the diagnostic utility of the clinically validated CA19.9 serum biomarker for oncology. J Nucl Med 2013;54:1876–82.
9. Girgis MD, Kenanova V, Olafsen T, McCabe KE, Wu AM, Tomlinson JS. Anti-CA19-9 diabody as a PET imaging probe for pancreas cancer. J Surg Res 2011;170:169–78.
10. Houghton JL, Membreno R, Abdel-Atti D, Cunanan KM, Carlin S, Scholz WW, et al. Establishment of the in vivo efficacy of pretargeted radioimmunotherapy utilizing inverse electron demand Diels-Alder click chemistry. Mol Cancer Ther 2017;16:124–33.
11. Houghton JL, Zeglis BM, Abdel-Atti D, Aggeler R, Sawada R, Agnew BJ, et al. Site-specifically labeled CA19.9-targeted immunoconjugates for the PET, NIRF, and multimodal PET/NIRF imaging of pancreatic cancer. Proc Natl Acad Sci U S A 2015;112:15850–5.
12. Houghton JL, Abdel-Atti D, Scholz WW, Lewis JS. Preloading with unlabeled CA19.9 targeted human monoclonal antibody leads to improved PET imaging with 89Zr-5B1. Mol Pharm 2017;14:908–15.
13. Ragupathi G, Damani P, Srivastava G, Srivastava O, Sucheck SJ, Ichikawa Y, et al. Synthesis of sialyl Lewis(a) (sLe (a), CA19-9) and construction of an immunogenic sLe(a) vaccine. Cancer Immunol Immunother 2009;58:1397–405.
14. Sawada R, Sun SM, Wu X, Hong F, Ragupathi G, Livingston PO, et al. Human monoclonal antibodies to sialyl-Lewis (CA19.9) with potent CDC, ADCC, and antitumor activity. Clin Cancer Res 2011;17:1024–32.
15. Vosjan MJ, Perk LR, Visser GW, Budde M, Jurek P, Kiefer GE, et al. Conjugation and radiolabeling of monoclonal antibodies with zirconium-89 for PET imaging using the bifunctional chelate p-isothiocyanatobenzyl-desferrioxamine. Nat Protoc 2010;5:739–43.
16. Holland JP, Sheh Y, Lewis JS. Standardized methods for the production of high specific-activity zirconium-89. Nucl Med Biol 2009;36:729–39.
17. Lindmo T, Bunn PA Jr. Determination of the true immunoreactive fraction of monoclonal antibodies after radiolabeling. Methods Enzymol 1986;121:678–91.
18. Naruki Y, Urita Y, Miyachi Y, Otsuka S, Noguchi M, Kogure T, et al. Radioimmunodetection of cancer of gastrointestinal tract and liver metastasis with I-131 anti-CEA and I-131 anti-CA19-9 monoclonal antibody cocktail (IMACIS-1). Ann Nucl Med 1994;8:163–9.
19. Baum RP, Lorenz M, Hottenrott C, Albrecht M, Senekowitsch R, Happ J, et al. Radioimmunoscintigraphy using monoclonal antibodies to CEA, CA 19-9 and CA 125. Int J Biol Markers 1988;3:177–84.
20. Strosberg J, El-Haddad G, Wolin E, Hendifar A, Yao J, Chasen B, et al. Phase 3 trial of (177)Lu-Dotatate for midgut neuroendocrine tumors. N Engl J Med 2017;376:125–35.
21. Hofman MS, Violet J, Hicks RJ, Ferdinandus J, Thang SP, Akhurst T, et al. [(177)Lu]-PSMA-617 radionuclide treatment in patients with metastatic castration-resistant prostate cancer (LuPSMA trial): a single-centre, single-arm, phase 2 study. Lancet Oncol 2018;19:825–33.
22. Fink DM, Steele MM, Hollingsworth MA. The lymphatic system and pancreatic cancer. Cancer Lett 2016;381:217–36.
23. Haab BB, Huang Y, Balasenthil S, Partyka K, Tang H, Anderson M, et al. Definitive characterization of CA 19-9 in resectable pancreatic cancer using

a reference set of serum and plasma specimens. PloS One 2015;10: e0139049.
24. Goldenberg DM, Nabi HA. Breast cancer imaging with radiolabeled antibodies. Semin Nucl Med 1999;29:41–8.
25. O'Donoghue JA, Lewis JS, Pandit-Taskar N, Fleming SE, Schöder H, Larson SM, et al. Pharmacokinetics, biodistribution, and radiation dosimetry for 89Zr-trastuzumab in patients with esophagogastric cancer. J Nucl Med 2018;59:161–6.
26. Ulaner GA, Lyashchenko SK, Riedl Ruan, Zanzonico PB, Lake D, et al. First-in-human human epidermal growth factor Receptor 2-targeted imaging using 89Zr-Pertuzumab PET/CT: dosimetry and clinical application in patients with breast cancer. Nucl Med 2018;59:900–6.
27. Pandit-Taskar N, O'Donoghue JA, Beylergil V, Lyashchenko S, Ruan S, Solomon SB, et al. ^{89}Zr-huJ591 immuno-PET imaging in patients with advanced metastatic prostate cancer. Eur J Nucl Med Mol Imaging 2014;41: 2093–105.
28. Deloar HM, Fujiwara T, Shidahara M, Nakamura T, Watabe H, Narita Y, Itoh M, Miyake M, Watanuki S. Estimation of absorbed dose for 2-[F-18]fluoro-2-deoxy-D-glucose using whole-body positron emission tomography and magnetic resonance imaging. Eur J Nucl Med 1998;25:565–74.
29. Cherry SR, Jones T, Karp JS, Qi J, Moses WW, Badawi RD. Total-body PET: maximizing sensitivity to create new opportunities for clinical research and patient care. J Nucl Med 2018;59:3–12.
30. Allen VB, Gurusamy KS, Takwoingi Y, Kalia A, Davidson BR. Diagnostic accuracy of laparoscopy following computed tomography (CT) scanning for assessing the resectability with curative intent in pancreatic and periampullary cancer. Cochrane Database Syst Rev 2016;7: CD009323.
31. Strobel O, Neoptolemos J, Jäger D, Büchler MW. Optimizing the outcomes of pancreatic cancer surgery. Nat Rev Clin Oncol 2019;16: 11–26.